

RESEARCH ARTICLE

Open Access



# Source apportionment of ambient PM<sub>2.5</sub> in Ho Chi Minh City, Vietnam

Ngoc Tran<sup>1\*</sup>, Yusuke Fujii<sup>1,2</sup>, Md Firoz Khan<sup>3</sup>, To Thi Hien<sup>4,5</sup>, Tran Hoang Minh<sup>4,5</sup>, Hiroshi Okochi<sup>6</sup> and Norimichi Takenaka<sup>1,2</sup>

## Abstract

The emission sources of fine particulate matter (PM<sub>2.5</sub>) have not yet been fully identified in Ho Chi Minh City (HCMC), Vietnam, presenting difficulties to authorities in controlling air pollution efficiently. To address this issue, this study explores the source apportionment of PM<sub>2.5</sub> by the positive matrix factorization (PMF) model and identifies potential regional sources through the weighted concentration-weighted trajectory (WCWT) model based on the field observation data of PM<sub>2.5</sub> in HCMC. 24-h PM<sub>2.5</sub> samples were collected in central HCMC for a year (September 2019–August 2020). Herein, inductively coupled plasma mass spectroscopy was used to analyze trace elements, in addition to identifying PM<sub>2.5</sub> mass and other chemical species, such as water-soluble ions and carbonaceous species, reported in our former study. The PMF results showed that PM<sub>2.5</sub> in HCMC was dominated by anthropogenic-rich sources comprising biomass burning, coal combustion, transportation, and crustal origins (36.4% of PM<sub>2.5</sub> mass), followed by secondary ammonium sulfate (18.4%), sea salt (13.7%), road dust (9.6%), and coal and crude oil combustion (9.4%). WCWT results suggested that the geological sources of PM<sub>2.5</sub> were mainly from local areas and scattered to the northeast/southwest of HCMC. In addition, the long-range transport of PM<sub>2.5</sub> from surrounding countries was revealed during the assembly restriction and lockdown period in 2020.

**Keywords** PM<sub>2.5</sub>, PMF, Source apportionment, Trace elements, Ho Chi Minh City, Vietnam

\*Correspondence:

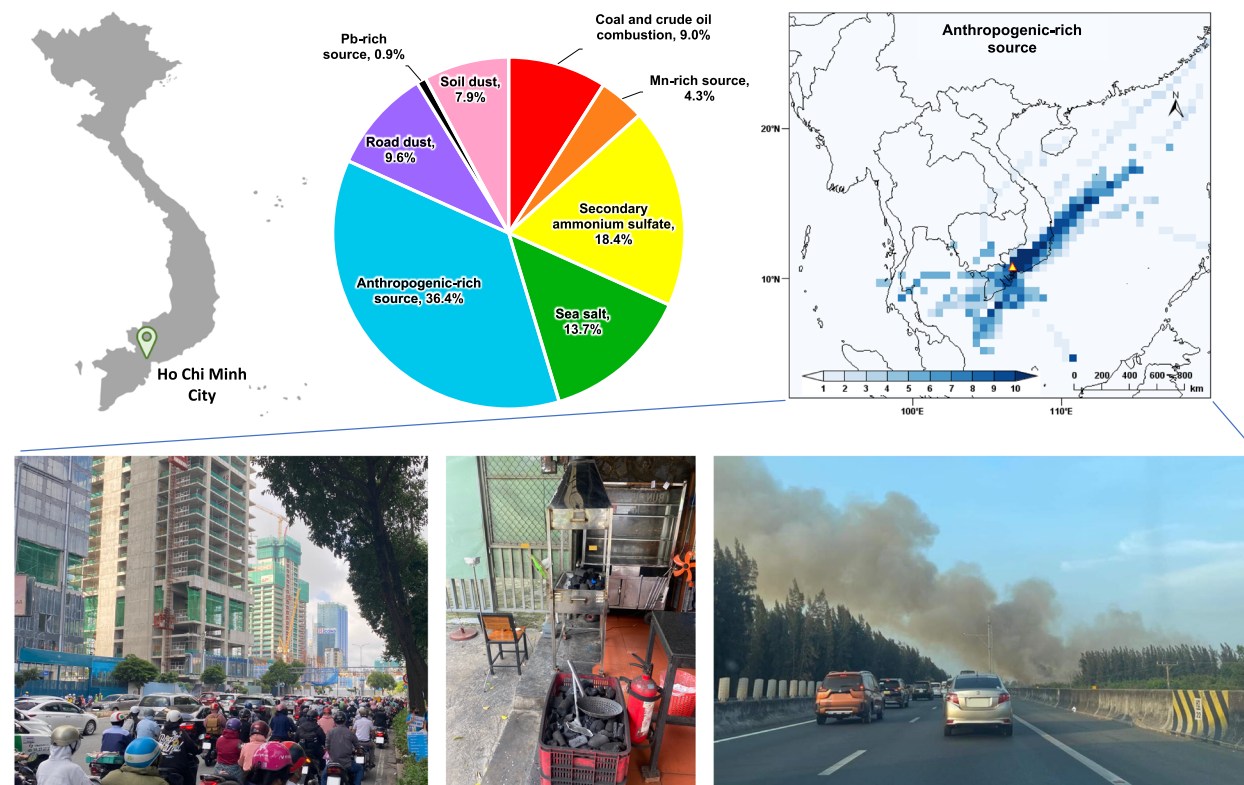
Ngoc Tran  
mdb04018@st.osakafu-u.ac.jp

Full list of author information is available at the end of the article



© The Author(s) 2023. **Open Access** This article is licensed under a Creative Commons Attribution 4.0 International License, which permits use, sharing, adaptation, distribution and reproduction in any medium or format, as long as you give appropriate credit to the original author(s) and the source, provide a link to the Creative Commons licence, and indicate if changes were made. The images or other third party material in this article are included in the article's Creative Commons licence, unless indicated otherwise in a credit line to the material. If material is not included in the article's Creative Commons licence and your intended use is not permitted by statutory regulation or exceeds the permitted use, you will need to obtain permission directly from the copyright holder. To view a copy of this licence, visit <http://creativecommons.org/licenses/by/4.0/>.

## Graphical Abstract



## 1 Introduction

Fine particulate matter (PM<sub>2.5</sub>) has become a serious air pollutant due to its negative effect on human health via prolonged exposure, visibility reduction, and climate change (Khan et al., 2016; Li et al., 2022). PM<sub>2.5</sub> with an aerodynamic diameter of less than 2.5 μm is emitted directly or formed via gas-to-particle conversion from various natural (e.g., forest fire, volcanic eruption, and sea salt) and anthropogenic sources (e.g., traffic emission, fuel combustion, and industrial processes) (Zhuang et al., 2017). Industrialization and urbanization in developing countries, especially in big cities, are responsible for high concentration and complex sources of PM<sub>2.5</sub> (Yang et al., 2018). Therefore, identifying the main sources of ambient PM<sub>2.5</sub> is crucial for policymakers to effectively implement strategies to reduce PM<sub>2.5</sub> levels.

Southeast Asia (SEA) is the third most populous region in the world, with most of the countries categorized as developing nations. Several studies regarding ambient PM<sub>2.5</sub> in SEA have shown the dominant contributions of biomass burning, coal combustion, and transportation (e.g., Fujii et al., 2016; Koplitz et al., 2017; Yin et al., 2019). However, understanding the primary sources of PM<sub>2.5</sub> in

Vietnam, the third most populous country in SEA remains elusive due to the lack of long-term field observation data. Ho Chi Minh City (HCMC) is a major city in Vietnam with the largest population density and is surrounded by numerous industrial zones. Road traffic emissions, shipping emissions, coal combustion, and industrial processes have been suggested as potential PM<sub>2.5</sub> sources in HCMC (Hien et al., 2022; Ho et al., 2020; Ho & Clappier, 2011; Huong Giang & Kim Oanh, 2014). However, relevant studies till now were conducted for short terms and/or did not focus on trace elements, which are generally considered to be reliable indicators of common PM<sub>2.5</sub> sources. For instance, previous studies have indicated that As and Pb represent coal combustion emissions, Ni and V suggest heavy oil combustion in shipping activities, K is a tracer of biomass burning, and Al and Ca originate from soil dust (Bressi et al., 2014; Khan et al., 2016; Taylor, 1964; Zong et al., 2018). Therefore, data on trace elements based on long-term field observation should be helpful for the accurate identification of emission sources in HCMC.

The positive matrix factorization (PMF) model has been widely used for source apportionment (Bressi et al.,

2014; Ledoux et al., 2017; Makkonen et al., 2023; Naye-bare et al., 2018; Taghvaei et al., 2018; Zong et al., 2018). Although it is a practical approach for source identification, the model requires a data set of over 100 samples and at least 10 analyzed chemical compositions (Norris et al., 2014). WCWT model can be used to visualize geological PM<sub>2.5</sub> sources based on PMF results. To the best of our knowledge, there have been few studies in Vietnam that have rigorously adhered to the PMF criteria and incorporated WCWT for geographical source attribution. This study aimed to identify (1) PM<sub>2.5</sub> sources in the center of HCMC using the PMF model and (2) the geological origins of each PM<sub>2.5</sub> source using the WCWT model.

## 2 Material and methods

### 2.1 Sampling site and sample collection

The location and methods for sampling were described in our former report (Tran et al., 2023). The sampling site was in Vietnam National University Ho Chi Minh City—University of Science (latitude/longitude: 10° 45′ 43.6″ N/106° 40′ 52.8″ E). The university is in an urban area, approximately 10 m away from a main street and ~300 m away from a major traffic circle in central HCMC. HCMC is surrounded by numerous industrial zones (e.g., food and beverage processing, leather manufacturing, plastic and rubber manufacturing, chemical manufacturing, and power plants) within a 20–50 km radius away from central HCMC (suburban HCMC, Binh Duong Province, Dong Nai Province, and Long An Province; General Statistics Office, 2021). In brief, 24-h PM<sub>2.5</sub> samples were collected on the rooftop of a twelve-story building, which is 49 m above the ground level, from September 19, 2019, to August 20, 2020. Two sets of PM<sub>2.5</sub> Impact samplers (SKC, Inc.) were employed to simultaneously collect ambient PM<sub>2.5</sub> on 47-mm polytetrafluoroethylene (PTFE) and quartz fiber filters for 24 h at a flow rate of 10 L min<sup>-1</sup>.

### 2.2 Chemical analyses

In our previous study, PM<sub>2.5</sub> mass, water-soluble inorganic ions (WSIs; Na<sup>+</sup>, NH<sub>4</sub><sup>+</sup>, K<sup>+</sup>, Cl<sup>-</sup>, NO<sub>3</sub><sup>-</sup>, and SO<sub>4</sub><sup>2-</sup>), organic carbons (OC), and elemental carbon (EC) were determined. Detailed analytical methods and results of those species were provided in our former report (Tran et al., 2023).

In this study, a quarter of each PTFE filter was used to quantify 11 trace elements (V, As, Pb, Mn, Ni, Cu, Zn, Fe, Ca, Mg, and Al) using inductively coupled plasma mass spectroscopy (ICP-MS) (Perkin Elmer, Model: NexION 2000). The filter samples were cut into small pieces for an extraction procedure. A microwave-assisted digestion system (Milestone Start D, Italy) was applied using

an acid mixture of 6 mL of 65% HNO<sub>3</sub> and 2 mL of 98% H<sub>2</sub>SO<sub>4</sub>. The acid mixture and the pieces of filter samples were added into a tetrafluoromethaxil (TFM) vessel. Then, the TFM vessels were tightly closed and placed in the safety shields in the microwave system. A two-step temperature program was followed, consisting of 15 min at 200°C and another 15 min at 110°C. After completion of microwave digestion for 30 min, the TFM vessels were cooled down and the extracted samples were filtered before dilution to 25 mL into the volumetric flask using deionized water. The samples were refrigerated at 4°C for further metal analysis using ICP-MS (Perkin Elmer, Model: NexION 2000, USA). ICP multi-element standard solution XIII (Merck, Germany) was used for external calibration plotting and quantification of the metals in the samples. The detailed procedure of trace metal analyses, including quality assurance and quality control, is described in Khan et al. (2016). The method detection limits (MDL; ng m<sup>-3</sup>) of V, As, Pb, Mn, Ni, Cu, Zn, Fe, Ca, Mg, and Al were 0.13, 0.08, 0.01, 0.1, 0.19, 0.13, 0.48, 45.65, 99.14, 65.41, and 18.81, respectively.

### 2.3 Positive matrix factorization

PMF is a receptor model that decomposes a matrix of sample data based on the number of samples collected over a certain time and measured chemical species to identify possible factor contributions and factor profiles of the target variables (Paatero & Tapper, 1994). The principle of PMF is to address the chemical mass balance by following Eq. (1):

$$X_{ij} = \sum_{k=1}^p g_{ik} f_{kj} + e_{ij} \quad (1)$$

where  $X_{ij}$  is the concentration of the  $j_{\text{th}}$  species in the  $i_{\text{th}}$  sample,  $p$  is the number of factors,  $g_{ik}$  is the contribution of the  $k_{\text{th}}$  factor to the  $i_{\text{th}}$  sample,  $f_{kj}$  is the fraction of the  $j_{\text{th}}$  species in the  $k_{\text{th}}$  source, and  $e_{ij}$  is the residual error related to the concentration of the  $j_{\text{th}}$  species in the  $i_{\text{th}}$  sample.

PMF output includes factor contributions and factor profiles that are obtained by minimizing an objective function  $Q$  as follows:

$$Q = \sum_{i=1}^n \sum_{j=1}^m \left[ \frac{x_{ij} - \sum_{k=1}^p g_{ik} f_{kj}}{u_{ij}} \right]^2 \quad (2)$$

where  $n$  is the number of samples,  $m$  is the number of species, and  $u_{ij}$  is the uncertainty of the  $j_{\text{th}}$  species in the  $i_{\text{th}}$  sample.

In this study, the PMF model version 5.0 (Norris et al., 2014) was used. The two data sets for PMF input (123 samples × 20 species) were prepared as follows. For the

concentration data file, the concentration of species below the MDL was set as MDL/2. For the uncertainty data file, the uncertainty (Unc) of species was calculated as  $\text{Unc} = 5/6 \times \text{MDL}$ , if the concentration is  $\leq \text{MDL}$  or  $\text{Unc} = \sqrt{(\text{Error Fraction} \times \text{concentration})^2 + (0.5 \times \text{MDL})^2}$ , or if the concentration is  $> \text{MDL}$ . The signal-to-noise ratio (S/N) is used for species categorization. Species with  $S/N > 5$  and  $S/N < 5$  are classified as “strong” and “weak,” respectively (Table S1) (Nayebare et al., 2018). S/N of  $\text{PM}_{2.5}$  mass, which is the total variable, was set as “weak” to reduce their strong impact on the model solution. Extra modeling uncertainty was set at 5% for all species to encompass the analytical, measurement, and modeling errors during analyses. Additionally, six to ten factors were examined to determine the optimal solution based on the explicability of the factor profiles in the base run and their high matching rate in the bootstrap run (Fujii et al., 2017). Bootstrap analysis was conducted with a block size of 10 with 100 bootstrap runs, and a minimum correlation value of 0.6 was used as the threshold for an acceptable run. The detailed PMF descriptions can be obtained elsewhere (Norris et al., 2014).

#### 2.4 Weighted concentration-weighted trajectory model

The WCWT model is an effective method for identifying source regions (Hsu et al., 2003). In this study, TrajStat software developed by Wang et al. (2009) was employed for WCWT analysis, which is reported in our former study (Tran et al., 2023). The air mass backward trajectories were calculated based on the Global Data Assimilation System data, and the corresponding  $\text{PM}_{2.5}$  mass contribution to the factors delineated by the PMF result (Table 1) was used as the WCWT input (Ali-Taleshi et al., 2021; Zong et al., 2018). The 72-h backward trajectories were calculated for each monitoring day using the TrajStat software at a height of 500 m above the ground level (Tran et al., 2023; Wang et al., 2009). Details on the WCWT, such as its definitions, formulas, and criteria, are available in previous reports (Hsu et al., 2003; Wang et al., 2009).

### 3 Results and discussion

HCMC is strongly affected by a monsoon-influenced tropical climate. The region has two distinct seasons: the dry season (December–April) and the rainy season (May–November). In late 2019, the COVID-19 pandemic spread globally. In line with the global response to the pandemic, Vietnam’s government declared various directives that restricted the immigration, movement, assembly, and national lockdown of citizens from February to April 2020 (i.e., during the dry season). As we described in Tran et al. (2023), the sampling periods in this study were categorized into four stages as follows:

- Stage 1 (September–November 2019): Rainy season before the assembly restriction and lockdown period (ARL)
- Stage 2 (December 2019–January 2020): Dry season before the ARL
- Stage 3 (February–April 2020): Dry season during the ARL
- Stage 4 (May–August 2020): Rainy season following the ARL

#### 3.1 Trace elements

The annual concentration of quantified elements was  $2.40 \pm 1.37 \mu\text{g m}^{-3}$  (average  $\pm$  standard deviation), accounting for  $8.4\% \pm 11.9\%$  of the  $\text{PM}_{2.5}$  mass. The statistical results of individual trace element concentrations are presented in Table 1, including  $\text{PM}_{2.5}$  mass and other chemical species concentrations. The order of the dominant trace elements, arranged based on their average concentrations, is as follows:  $\text{Al} > \text{Ca} > \text{Fe} > \text{Mg} > \text{Zn} > \text{Cu} > \text{Mn} > \text{Ni} > \text{Pb} > \text{V} > \text{As}$ .

Enrichment factors (EFs) are widely used to approximately estimate the trace element sources (e.g., Fujii et al., 2016; Khan et al., 2016; Reimann & De Caritat, 2000). The EF for each of the trace elements was calculated using the following Eq. (3):

$$\text{EF} = \frac{([X]/[Al])_{\text{Air}}}{([X]/[Al])_{\text{Crust}}} \quad (3)$$

where  $([X]/[Al])_{\text{Air}}$  and  $([X]/[Al])_{\text{Crust}}$  are the mass ratios of a given metal ( $X$ ) to Al in  $\text{PM}_{2.5}$  and crust, respectively. The reference crust data reported by Taylor (1964) was used to calculate  $([X]/[Al])_{\text{Crust}}$ . Al was used as a reference element due to its abundance in the Earth’s crust (Nayebare et al., 2018). Previous studies reported that  $\text{EF} > 10$  suggests a strong contribution of anthropogenic sources to trace metals, while  $\text{EF} < 10$  indicates that the primary contributor is the Earth’s crust (e.g., Fujii et al., 2016; Khan et al., 2016; Reimann & De Caritat, 2000). In this study, the EFs of Cu, As, and Zn were above 10, suggesting human activities to be predominantly responsible for their occurrence (Fig. 1a), while the EFs of Fe, Ca, Mg, V, and Mn were below 10, indicating that their enrichment occurred from the Earth’s crust. The EFs of Ni and Pb were close to 10, implying similar contributions from natural and anthropogenic sources. In Stage 3, the EF value of Zn, As, and Pb decreased, while EF values of Ni increased (Fig. 1b). This discrepancy also leads to the different contribution of  $\text{PM}_{2.5}$  sources, which is discussed in Section 3.2.

The total concentration of crustal elements (Al, Fe, Ca, Mg, V, and Mn) ranged from 0.30 to  $6.59 \mu\text{g m}^{-3}$

**Table 1** Statistical concentration of PM<sub>2.5</sub> and chemical species

Species	Whole period			Stage 1 (Sep–Nov)			Stage 2 (Dec–Jan)			Stage 3 (Feb–Apr)			Stage 4 (May–Aug)		
	Avg <sup>a</sup> ± Std <sup>b</sup>	Min	Max	Avg ± Std	Min	Max									
PM <sub>2.5</sub> (µg m <sup>-3</sup> )	28.44 ± 11.55	24.42	60.91	41.09 ± 12.14	23.70	61.94	24.52 ± 8.83	12.25	43.97	21.55 ± 7.33	9.570	39.345	21.55 ± 7.33	9.570	39.345
Cl <sup>-</sup> (µg m <sup>-3</sup> )	0.38 ± 0.27	0.02	0.88	0.7 ± 0.31	0.27	1.40	0.46 ± 0.13	0.27	0.78	0.3 ± 0.23	0.02	1.10	0.3 ± 0.23	0.02	1.10
NO <sub>3</sub> <sup>-</sup> (µg m <sup>-3</sup> )	1.12 ± 0.75	0.59	3.41	2 ± 1.15	0.34	5.06	0.86 ± 0.38	0.34	1.66	0.83 ± 0.48	0.07	2.45	0.83 ± 0.48	0.07	2.45
SO <sub>4</sub> <sup>2-</sup> (µg m <sup>-3</sup> )	3.26 ± 1.95	2.32	8.77	4.57 ± 2.91	1.66	11.80	2.68 ± 0.98	1.47	6.73	1.98 ± 0.85	0.77	4.18	1.98 ± 0.85	0.77	4.18
Na <sup>+</sup> (µg m <sup>-3</sup> )	0.44 ± 0.27	0.18	1.33	0.74 ± 0.3	0.29	1.24	0.53 ± 0.2	0.25	1.02	0.23 ± 0.11	0.06	0.62	0.23 ± 0.11	0.06	0.62
NH <sub>4</sub> <sup>+</sup> (µg m <sup>-3</sup> )	0.91 ± 0.71	0.38	2.67	1.54 ± 1.18	0.25	4.13	0.72 ± 0.42	0.20	2.56	0.54 ± 0.33	0.09	1.70	0.54 ± 0.33	0.09	1.70
K <sup>+</sup> (µg m <sup>-3</sup> )	0.8 ± 0.54	0.00	2.79	1.06 ± 0.41	0.42	1.80	0.52 ± 0.34	0.15	1.52	0.65 ± 0.47	0.09	2.09	0.65 ± 0.47	0.09	2.09
OC (µg m <sup>-3</sup> )	8.77 ± 4.02	8.00	22.46	11.81 ± 2.7	8.05	17.04	6.45 ± 3.25	3.17	15.35	6.77 ± 2.34	2.09	11.18	6.77 ± 2.34	2.09	11.18
EC (µg m <sup>-3</sup> )	2.82 ± 1.53	2.15	8.80	3.54 ± 0.87	2.16	5.19	1.78 ± 0.95	0.90	4.22	2.24 ± 1.09	0.41	5.56	2.24 ± 1.09	0.41	5.56
Trace elements (µg m <sup>-3</sup> )	2.40 ± 1.37	0.36	4.51	2.74 ± 1.26	0.81	4.82	3.01 ± 1.67	0.61	6.64	1.69 ± 0.85	0.36	3.38	1.69 ± 0.85	0.36	3.38
V (ng m <sup>-3</sup> )	0.73 ± 0.54	0.47	2.75	1.00 ± 0.39	0.40	1.59	0.5 ± 0.24	0.10	1.07	0.43 ± 0.4	0.09	1.69	0.43 ± 0.4	0.09	1.69
As (ng m <sup>-3</sup> )	0.27 ± 0.24	0.08	1.08	0.37 ± 0.21	0.10	0.88	0.14 ± 0.15	0.03	0.76	0.19 ± 0.2	0.00	1.02	0.19 ± 0.2	0.00	1.02
Pb (ng m <sup>-3</sup> )	0.87 ± 0.84	0.14	3.67	0.91 ± 0.88	0.07	3.05	0.56 ± 0.64	0.01	2.44	0.81 ± 0.72	0.09	2.80	0.81 ± 0.72	0.09	2.80
Mn (ng m <sup>-3</sup> )	5.46 ± 4.37	0.63	15.94	2.42 ± 0.99	0.94	4.35	5.03 ± 4.22	0.42	14.11	7.03 ± 4.93	0.37	17.52	7.03 ± 4.93	0.37	17.52
Ni (ng m <sup>-3</sup> )	4.09 ± 5.49	0.03	9.09	1.22 ± 2.57	0.14	10.96	7.86 ± 6.95	0.06	23.26	3.74 ± 5.42	0.05	20.85	3.74 ± 5.42	0.05	20.85
Cu (ng m <sup>-3</sup> )	8.13 ± 5.86	0.06	20.60	9.05 ± 3.4	3.31	16.86	10.71 ± 5.58	0.12	22.58	7.64 ± 6.62	0.14	23.43	7.64 ± 6.62	0.14	23.43
Zn (ng m <sup>-3</sup> )	11.66 ± 10.35	1.97	39.56	16.61 ± 10.07	0.55	37.59	9.42 ± 9.93	0.17	31.15	7.14 ± 7.32	0.10	28.98	7.14 ± 7.32	0.10	28.98
Fe (ng m <sup>-3</sup> )	501.68 ± 473.15	15.72	2002.94	579.58 ± 499.39	51.49	1862.44	635.72 ± 542.19	36.25	1846.47	376.84 ± 323.4	20.54	1127.56	376.84 ± 323.4	20.54	1127.56
Ca (ng m <sup>-3</sup> )	683.79 ± 506.49	67.87	1674.82	802.56 ± 519.41	99.22	1880.79	871.5 ± 605.42	78.80	2340.03	460.22 ± 332.43	10.58	970.19	460.22 ± 332.43	10.58	970.19
Mg (ng m <sup>-3</sup> )	445.05 ± 280.48	35.47	1133.59	471.4 ± 243.47	48.42	982.27	529.76 ± 314.95	43.57	1192.40	332.21 ± 225.01	30.96	729.36	332.21 ± 225.01	30.96	729.36
Al (ng m <sup>-3</sup> )	741.17 ± 427.53	206.07	1541.86	856.81 ± 367.94	266.48	1601.61	942.38 ± 539.59	182.38	2233.01	507.06 ± 248.38	107.04	980.59	507.06 ± 248.38	107.04	980.59

<sup>a</sup> Average concentration, <sup>b</sup>Standard deviation

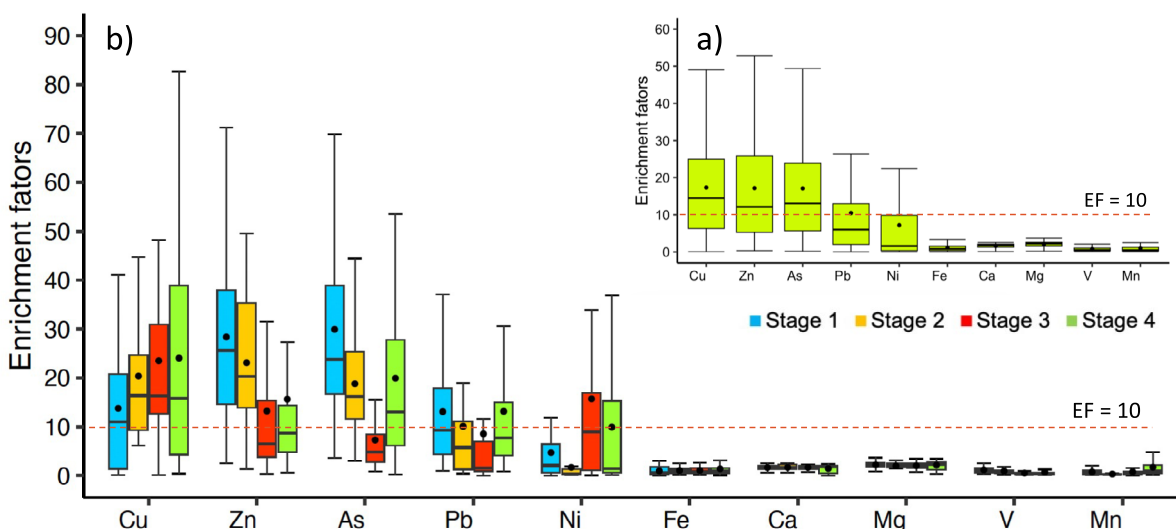


**Fig. 1** Box-and-whisker plot of EFs for trace elements in PM<sub>2.5</sub> on HCMC by (a) the whole sampling period and (b) stages. Black dots in center boxes indicate the mean value of EFs. Horizontal lines of boxes indicate the median value, 25th and 75th percentiles, and whiskers indicate the 10th and 90th percentiles

( $2.37 \pm 1.37 \mu\text{g m}^{-3}$ ), which accounted for 82–99% of the total trace elements (Table 1). Thus, crustal sources were major sources of trace elements in ambient PM<sub>2.5</sub> in HCMC. Non-crustal elements, such as Cu, As, and Zn, were minor elements; however, they are important indicators of anthropogenic sources. Cu and Zn are closely related to vehicular and industrial sources, while As is indicative of emissions from coal combustion (Nayebare et al., 2018; Zhao & Luo, 2018). Source identification based on trace elements is discussed in Section 3.2.

### 3.2 Source identification

A PM<sub>2.5</sub> data set of dimensions 123 samples  $\times$  20 species (PM<sub>2.5</sub> mass, Cl<sup>-</sup>, NO<sub>3</sub><sup>-</sup>, SO<sub>4</sub><sup>2-</sup>, Na<sup>+</sup>, NH<sub>4</sub><sup>+</sup>, K<sup>+</sup>, OC, EC, V, As, Pb, Mn, Ni, Cu, Zn, Fe, Ca, Mg, and Al) with model results of 6–10 factors were assessed using PMF. The uncertainty of the factors was examined by bootstrapping (BS) and displacement (DISP) methods. The solution with eight factors was stable, where all factors could be mapped from 99 to 100% in the BS run, and no swaps were recorded in the DISP analysis. Moreover, factors in other solutions were mapped to only 90% or lower in the BS trial (Table S2). Therefore, the 8-factor solution was deemed to be the optimal solution in this study. The statistical result calculated using PMF, including mean, minimum, and maximum values, SD, and S/N of the 19 species by eight factors is displayed in Table S1. Figure 2 presents the source profiles of PM<sub>2.5</sub> in HCMC estimated using the PMF model. Figure S2 shows the regression coefficients between measured and PMF-estimated PM<sub>2.5</sub> concentration. The percent contributions of each factor

and corresponding concentrations are presented in Fig. 3. The time series of PM<sub>2.5</sub> concentration ( $\mu\text{g m}^{-3}$ ) by each source are shown in Fig. S3.

#### 3.2.1 Anthropogenic-rich source

This source is characterized by high loadings of K<sup>+</sup>, OC, EC, NO<sub>3</sub><sup>-</sup>, Fe, As, and V (Fig. 2); it contributed to 36.4% of the total PM<sub>2.5</sub> mass during the sampling period. OC and EC contributed to  $40.4 \pm 8.9\%$  of the PM<sub>2.5</sub> mass and showed a high correlation with K<sup>+</sup> (Table 2,  $r > 0.78$ ,  $p < 0.01$ ). K<sup>+</sup> is generally known as a biomass burning tracer. Additionally, As is closely related to coal combustion activities (Cui et al., 2020; Zhao & Luo, 2018), and it showed a moderate correlation with K<sup>+</sup>, OC, and EC (Table 2). Thus, it could be inferred that As, K<sup>+</sup>, OC, and EC originated from a common emission source. NO<sub>3</sub><sup>-</sup> is known as a common pollutant from vehicular emissions (Xue et al., 2014), and it is the second most abundant WSIs in HCMC (Tran et al., 2023). In line with previous studies, in HCMC, NO<sub>3</sub><sup>-</sup> is attributed to vehicular emissions (Ho et al., 2020) and biomass burning emissions (Huy et al., 2022). Similarly, in this study, NO<sub>3</sub><sup>-</sup> showed a moderate correlation with K<sup>+</sup>, OC, and EC (Table 2), implying that the influence of biomass burning on NO<sub>3</sub><sup>-</sup> could not be neglected. The EFs of Fe and V indicated the influence of the Earth’s crust, as discussed in Section 3.1. Collectively, this factor features characteristics indicating mixed sources of biomass burning, coal combustion, transportation, and crustal origins (hereafter “anthropogenic-rich source”). For PMF calculation, to separately extract these sources in the anthropogenic-rich source,

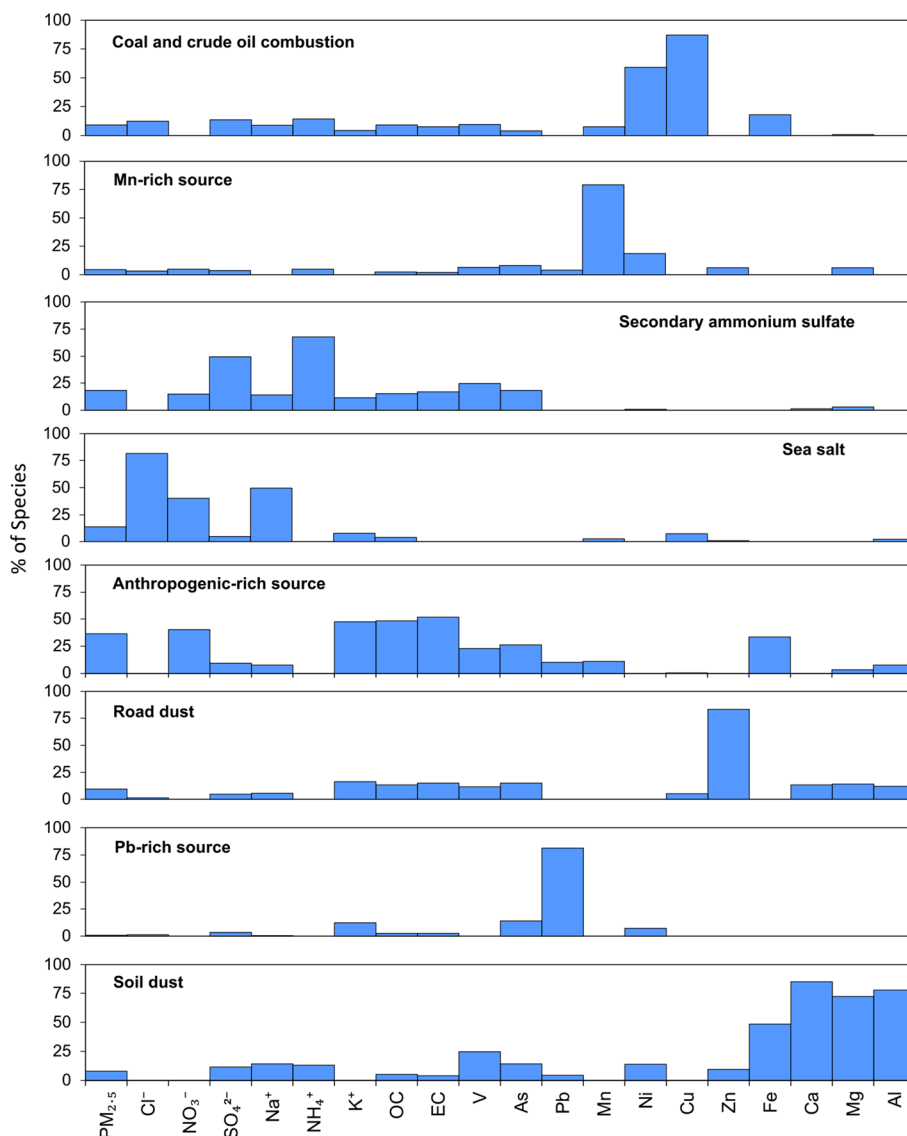


**Fig. 2** Profiles of eight factors extracted by PMF

data of additional individual source indicators (e.g., levoglucosan for biomass burning, and polycyclic aromatic hydrocarbons such as chrysene, benzo(k)fluoranthene, and indeno(1,2,3-cd) pyrene for traffic exhaust, phenanthrene and anthracene for coal combustion) would be required.

Contributions of the anthropogenic-rich source to the PM<sub>2.5</sub> mass during different stages (average μg m<sup>-3</sup>, %) are as follows: Stage 1 (15.49 μg m<sup>-3</sup>, 42.5%), Stage 2 (11.58 μg m<sup>-3</sup>, 30.8%), Stage 3 (5.42 μg m<sup>-3</sup>, 17.8%), and Stage 4 (9.49 μg m<sup>-3</sup>, 42.2%) (Figs. 3 and S1). The lower contribution of anthropogenic-rich source during Stage 2 as compared to Stage 1 is attributed to the dry deposition of EC and intensive photochemical transformation

of OC in the dry season (Tran et al., 2023). During Stage 3, the contribution of the anthropogenic-rich source to the PM<sub>2.5</sub> mass decreased by approximately 53% as compared to Stage 2 (Fig. 3). The concentration of OC, EC, and K<sup>+</sup> (Table 1) and EF values of As (Fig. 1b) also displayed significant reduction during Stage 3, which could be attributed to a reduction in emissions from local activities during the ARL (Tran et al., 2023). Thus, it can be inferred that the anthropogenic-rich source comprising biomass burning, coal combustion, transportation, and crustal origins may mainly be present at the local scale in HCMC. Various studies have reported an improvement in air quality in urban areas due to the COVID-19 restriction (Cui et al., 2020; Jeong et al., 2022;

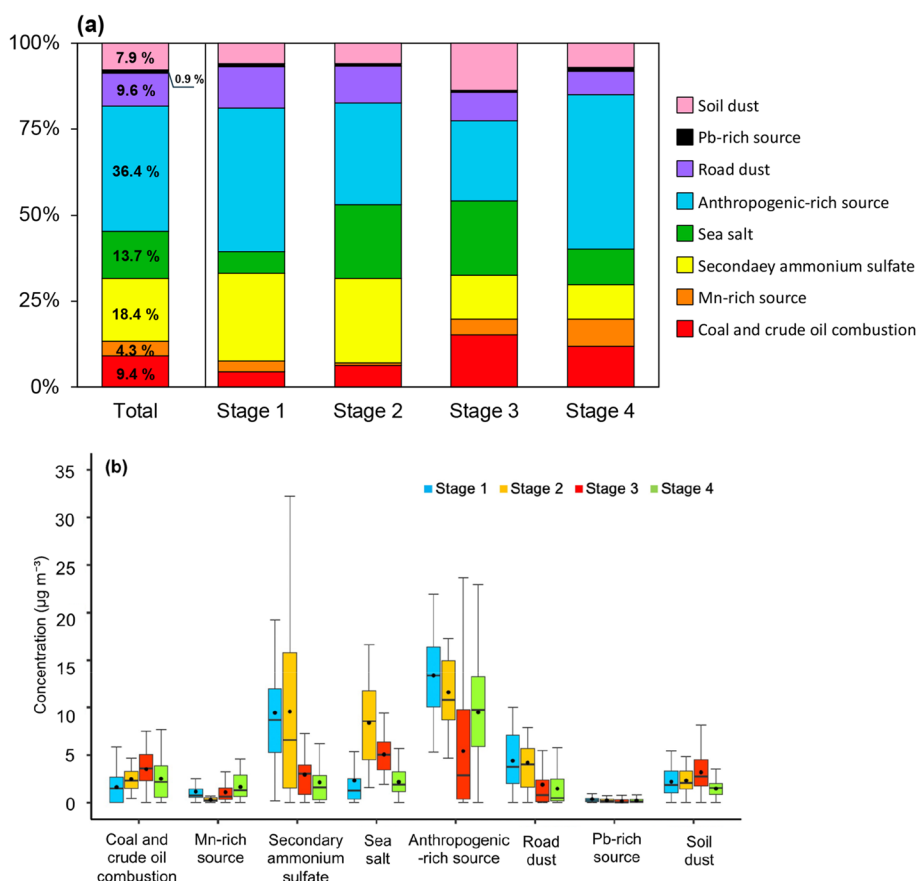


**Fig. 3** The contribution of each source to PM<sub>2.5</sub> (a) by percentage and (b) by concentration. Box-and-whisker plot for the source contribution to PM<sub>2.5</sub> concentration by stages, in which black dots in center boxes indicate mean values of EF, horizontal lines of boxes indicate median values, 25th and 75th percentiles, and whiskers indicate the 10th and 90th percentiles

Nguyen et al., 2022). The increased PM<sub>2.5</sub> concentrations contributed by the anthropogenic-rich source were also observed during Stage 4, suggesting that local emissions rebounded after the lockdown period. Because coal combustion has been identified as a local source, charcoal combustion for cooking activities may be a cause of PM<sub>2.5</sub> emissions in urban HCMC. The sampling site is surrounded by various conventional vendors and restaurants that use charcoal for boiling and grilling food. Thus, charcoal consumption should be taken into consideration while attempting to reduce direct local emissions in HCMC.

### 3.2.2 Secondary ammonium sulfate

Secondary ammonium sulfate (SAS) is represented by high loadings of NH<sub>4</sub><sup>+</sup> (67.8%) and SO<sub>4</sub><sup>2-</sup> (49.6%) (Chen et al., 2019; Long et al., 2014). SO<sub>4</sub><sup>2-</sup> was the most abundant species among the WSIs (~45%) in HCMC during the sampling period (Tran et al., 2023). The favorable formation of SAS in HCMC could be due to the high ambient temperatures in this region, as reported by earlier

studies (Huy et al., 2020, 2022). The NO<sub>3</sub><sup>-</sup>/SO<sub>4</sub><sup>2-</sup> ratio was 0.38 ± 0.19, indicating the dominant role of emissions from stationary sources (e.g., charcoal combustion and/or coal-fired thermal plants) to the urban atmosphere in HCMC (Tran et al., 2023). Sulfate particles are also released directly during the wet process of desulfurization in coal-fired thermal plants (Liu et al., 2017). SAS is generally associated with the “aging” of air pollution due to the slow oxidation of SO<sub>2</sub> to SO<sub>4</sub><sup>2-</sup> (Manoussakas et al., 2017), indicating that SAS may originate from long-range transport (Bressi et al., 2014; Makkonen et al., 2023). Luong et al. (2022) reported that SO<sub>4</sub><sup>2-</sup> is related to the long-range transport of coal combustion emissions (e.g., from coal-fired power plants, cement, and steel plants) in Vietnam. In addition, the presence of other species (As, OC, EC, K<sup>+</sup>, and NO<sub>3</sub><sup>-</sup>) and moderate correlation between SO<sub>4</sub><sup>2-</sup> and these species (Table 1, *r* > 0.5, *p* < 0.01) suggest a partial influence of the anthropogenic-rich source on the SAS formation.

The SAS source accounted for 18% of the PM<sub>2.5</sub> mass. The contribution of this source decreased during the

**Table 2** Correlation of PM<sub>2.5</sub> and chemical species

	PM <sub>2.5</sub>	Cl <sup>-</sup>	NO <sub>3</sub> <sup>-</sup>	SO <sub>4</sub> <sup>2-</sup>	Na <sup>+</sup>	NH <sub>4</sub> <sup>+</sup>	K <sup>+</sup>	OC	EC	V	As	Pb	Mn	Ni	Cu	Zn	Fe	Ca	Mg	Al
PM <sub>2.5</sub>	--																			
Cl <sup>-</sup>	0.421 <sup>b</sup>	--																		
NO <sub>3</sub> <sup>-</sup>	0.784 <sup>b</sup>	0.629 <sup>b</sup>	--																	
SO <sub>4</sub> <sup>2-</sup>	0.752 <sup>b</sup>	0.187 <sup>a</sup>	0.538 <sup>b</sup>	--																
Na <sup>+</sup>	0.588 <sup>b</sup>	0.622 <sup>b</sup>	0.533 <sup>b</sup>	0.427 <sup>b</sup>	--															
NH <sub>4</sub> <sup>+</sup>	0.677 <sup>b</sup>	0.233 <sup>b</sup>	0.570 <sup>b</sup>	0.910 <sup>b</sup>	0.346 <sup>b</sup>	--														
K <sup>+</sup>	0.736 <sup>b</sup>	0.261 <sup>b</sup>	0.570 <sup>b</sup>	0.541 <sup>b</sup>	0.360 <sup>b</sup>	0.359 <sup>b</sup>	--													
OC	0.884 <sup>b</sup>	0.171	0.663 <sup>b</sup>	0.659 <sup>b</sup>	0.403 <sup>b</sup>	0.561 <sup>b</sup>	0.782 <sup>b</sup>	--												
EC	0.824 <sup>b</sup>	0.148	0.648 <sup>b</sup>	0.637 <sup>b</sup>	0.328 <sup>b</sup>	0.500 <sup>b</sup>	0.809 <sup>b</sup>	0.918 <sup>b</sup>	--											
V	0.453 <sup>b</sup>	0.022	0.364 <sup>b</sup>	0.511 <sup>b</sup>	0.247 <sup>b</sup>	0.432 <sup>b</sup>	0.245 <sup>b</sup>	0.405 <sup>b</sup>	0.454 <sup>b</sup>	--										
As	0.577 <sup>b</sup>	0.029	0.398 <sup>b</sup>	0.524 <sup>b</sup>	0.154	0.401 <sup>b</sup>	0.614 <sup>b</sup>	0.589 <sup>b</sup>	0.670 <sup>b</sup>	0.512 <sup>b</sup>	--									
Pb	0.282 <sup>b</sup>	0.097	0.252 <sup>b</sup>	0.267 <sup>b</sup>	0.05	0.147	0.554 <sup>b</sup>	0.362 <sup>b</sup>	0.392 <sup>b</sup>	0.101	0.483 <sup>b</sup>	--								
Mn	-0.131	-0.177	-0.184 <sup>a</sup>	-0.078	-0.269 <sup>b</sup>	-0.096	-0.089	-0.125	-0.066	-0.036	0.059	0.112	--							
Ni	-0.181 <sup>a</sup>	0.069	-0.210 <sup>a</sup>	-0.114	0	-0.125	-0.192 <sup>a</sup>	-0.229 <sup>a</sup>	-0.234 <sup>b</sup>	-0.118	-0.123	-0.075	0.222 <sup>a</sup>	--						
Cu	-0.073	0.237 <sup>b</sup>	-0.076	-0.108	0.161	-0.073	-0.142	-0.143	-0.209 <sup>a</sup>	-0.112	-0.076	-0.109	0.299 <sup>b</sup>	0.467 <sup>b</sup>	--					
Zn	0.421 <sup>b</sup>	0.201 <sup>a</sup>	0.258 <sup>b</sup>	0.318 <sup>b</sup>	0.314 <sup>b</sup>	0.214 <sup>a</sup>	0.479 <sup>b</sup>	0.435 <sup>b</sup>	0.455 <sup>b</sup>	0.264 <sup>b</sup>	0.479 <sup>b</sup>	0.367 <sup>b</sup>	0.098	-0.104	0.123	--				
Fe	0.125	0.085	0.174	-0.019	0.224 <sup>a</sup>	-0.06	0.049	0.086	0.096	0.111	0.041	-0.097	-0.075	-0.003	0.048	-0.131	--			
Ca	0.114	0.181 <sup>a</sup>	0.092	0.132	0.297 <sup>b</sup>	0.087	0.025	-0.007	0.042	0.219 <sup>a</sup>	0.138	-0.057	-0.097	-0.035	-0.072	0.186 <sup>a</sup>	0.157	--		
Mg	0.122	0.124	0.07	0.148	0.238 <sup>b</sup>	0.087	0.058	-0.005	0.08	0.218 <sup>a</sup>	0.151	-0.059	-0.037	-0.027	-0.036	0.204 <sup>a</sup>	0.135	0.895 <sup>b</sup>	--	
Al	0.180 <sup>a</sup>	0.199 <sup>a</sup>	0.147	0.137	0.369 <sup>b</sup>	0.065	0.084	0.06	0.106	0.233 <sup>b</sup>	0.169	-0.05	-0.09	-0.011	-0.037	0.187 <sup>a</sup>	0.398 <sup>b</sup>	0.942 <sup>b</sup>	0.852 <sup>b</sup>	--

<sup>b</sup> Correlation is significant at the 0.01 level (two-tailed)

<sup>a</sup> Correlation is significant at the 0.05 level (two-tailed)

different sampling periods as follows: Stage 1 (27%), Stage 2 (20%), Stage 3 (13%), and Stage 4 (9%) (Fig. 3). The formation of SAS is strongly dependent on temperature (T) and relative humidity (RH) (Long et al., 2014; Xue et al., 2014), which varied within a narrow range ( $T = 29.1 \pm 1.0$  °C and  $RH = 69.7 \pm 4.1\%$ ) during the sampling period. Thus, the influence of meteorological factors on SAS formation could be neglected. The generation of electricity by coal-fired thermal plants was reduced due to the ARL (Tran et al., 2023), which can explain the decreasing trend of the contribution of SAS to the  $PM_{2.5}$  mass.

### 3.2.3 Sea salt

Sea salt is represented by high loadings of  $Cl^-$  (81.7 %) and  $Na^+$  (49.7%). Fresh sea salt is characterized by  $Cl^-$  and

$Na^+$  (Dai et al., 2013), while aged sea salt is characterized by  $SO_4^{2-}$ ,  $Mg^{2+}$ , and  $NH_4^+$  (Zhang et al., 2021). Thus, this factor is identified to be fresh sea salt, which contributed to 18.4% of the total  $PM_{2.5}$  mass in HCMC. The contribution of fresh sea salt was higher in dry seasons (Stages 2 and 3) than in rainy seasons (Stages 1 and 4) (Figs. 3b and 4), which could be due to wet deposition (Tran et al., 2023).

The molar ratio of  $Cl^-$  to  $Na^+$  ( $Cl^-/Na^+$ ) during the sampling period ranged from 0.04 to 2.99 with an average value of  $0.63 \pm 0.47$ . Figure S4 shows the time series of variations in  $Cl^-/Na^+$  molar ratios. In most cases, the  $Cl^-/Na^+$  molar ratio values were lower than those in bulk water (1.18), suggesting that chlorine depletion occurred during transport (Boreddy et al., 2014; Farren

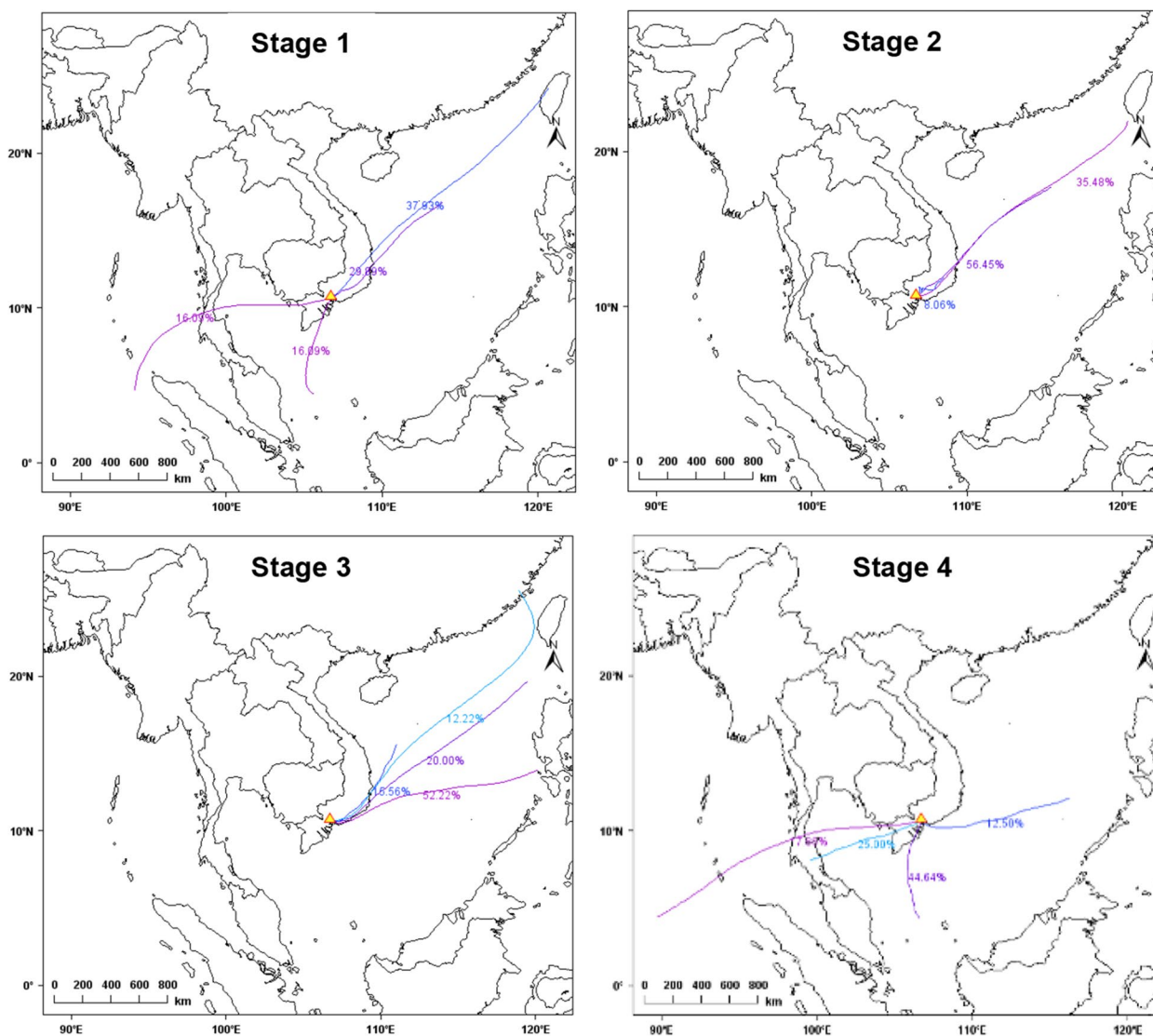


Fig. 4 Analytical clusters of 72 h backward trajectories to the sampling site at 500 m elevation by stages

et al., 2019). The high values of  $\text{Cl}^-/\text{Na}^+$  molar ratios in May and June imply an additional source of  $\text{Cl}^-$  during this period. Previous studies have reported that May–June is a period of open burning of rice straw in south-western HCMC and increased the  $\text{PM}_{2.5}$  concentration in urban HCMC (Hien et al., 2019; Huy et al., 2022).  $\text{Cl}^-$  is a major ion from maize residue and rice straw burning in SEA (Hong Phuong et al., 2022; Khamkaew et al., 2016). Therefore, the influence of open burning in May–June from the Mekong Delta on air quality in HCMC could not be neglected, which is further validated by the high concentration of  $\text{K}^+$  in May–June and higher correlations of  $\text{Cl}^-$  with  $\text{K}^+$ , OC, and EC observed during Stage 4 (Tran et al., 2023).

### 3.2.4 Road dust

The major presence of Zn (83.4%) was the predominant reason to classify this factor as road dust. As mentioned in Section 3.1, high EF values of Zn imply their derivation from anthropogenic activities. In SEA countries, Zn is generated from diesel and two-stroke vehicles and road dust (Dahari et al., 2019), tires, motor oil, and motor vehicle brakes (Alias et al., 2020; Khan et al., 2016). In Vietnam, Zn has been reported to be the most abundant element in ambient air, and it constitutes a large portion of road dust (Bui et al., 2023; Hien et al., 2022; Makkonen et al., 2023). In addition, the minor contributions (< 17%) of  $\text{K}^+$ , OC, EC, V, As, Cu, Ca, Mg, and Al to this factor suggest the fractional contribution of anthropogenic-rich sources and crustal origins. Therefore, this factor is identified as road dust and is related to vehicular emissions.

The seasonal variation of  $\text{PM}_{2.5}$  attributed to road dust was not observed in this study.  $\text{PM}_{2.5}$  mass in the rainy season was comparable with the dry season (Stage 1,  $4.41 \pm 3.05 \mu\text{g m}^{-3}$ ; Stage 2,  $4.19 \pm 3.1 \mu\text{g m}^{-3}$ ; Stage 3,  $1.9 \pm 2.51 \mu\text{g m}^{-3}$ ; and Stage 4,  $1.47 \pm 1.88 \mu\text{g m}^{-3}$ ). Although heavy rain could reduce a high amount of water-soluble pollutants present in the atmosphere, the solubility of Zn in water depends more on the acid strength of rain by volume and on the size distribution of Zn in the PM (Gunawardena et al., 2013; Hu & Balasubramanian, 2003). Herein, neither the pH value of rainwater during the sampling period nor the size distribution of Zn was analyzed. Therefore, the variation of  $\text{PM}_{2.5}$  attributed to road dust could not be explained.

In Stage 3, the EFs of Zn were reduced (Fig. 1b), indicating a reduction in Zn emission owing to anthropogenic activities. The  $\text{PM}_{2.5}$  from road dust was reduced by ~55% from Stage 2 to Stage 3, attributing this fall to the reduction of transportation in local areas because of the ARL. The contribution of road dust continued to decrease during Stage 4 regardless of the resumption of work in the post-lockdown period. This result is

consistent with other studies, indicating a similar reduction of road dust emissions before and after the lockdown (Cui et al., 2020; Makkonen et al., 2023; Nguyen et al., 2022).

### 3.2.5 Coal and crude oil combustion

This factor featured a high loading of Cu (87%) and Ni (59%), tentatively defined as “Cu- and Ni-rich factor”. The EF values of Cu were above 10, implying that it was derived from anthropogenic activities during the entire sampling period. Cu is emitted from diesel combustion, brake lining wear, and nonexhaust road dust, which are identified as local emissions (Cui et al., 2020). The EFs of Ni were higher during Stages 3 and 4, as compared to during Stages 1 and 2 (Fig. 1b), implying dominant emission from anthropogenic activities during Stages 3 and 4, which were ARL and post-ARL periods. Ni is known as a tracer of shipping emissions (combustion of heavy oil) (Alias et al., 2020; Hien et al., 2022), which is one of the main sources of  $\text{PM}_{2.5}$  in Vietnam (Bui et al., 2023; Hien et al., 2022; Huyen et al., 2022; Makkonen et al., 2023). However, the highest concentrations of Cu and Ni were observed during Stage 3 (Table 1), demonstrating a contradiction with the local sources (anthropogenic-rich source and road dust). Therefore, Cu and Ni were not primarily derived from local sources.

The high concentration levels of both Cu and Ni were obtained from the burning of coal and oil (Wang et al., 2021). Previous studies applied the V/Ni ratio as the diagnostic criterion for oil combustion, where the value of the ratio between 2 and 4 represents the combustion of heavy oil, and a value of < 2 represents the combustion of gasoline and diesel (Hao et al., 2018; Makkonen et al., 2023; Manousakas et al., 2017). Meanwhile, the V/Ni ratio < 1 represents various types of crude oils with a high content of Ni and a low content of V in China (Chifang et al., 1991; Hao et al., 2018). In this study, the V/Ni ratio governed by Cu- and Ni-rich factors was 0.04, which was comparable to those in Chifeng, China (Hao et al., 2018). Therefore, the low ratios of V/Ni indicate that Ni emission in HCMC was associated with crude oil emission. Cu is known to be one of the main elements released into the atmosphere from industrial coal combustion in southeast China (Li et al., 2017), residential coal combustion (Yan et al., 2022), and vehicular exhaust (Liu et al., 2017). Based on the variation of  $\text{PM}_{2.5}$  governed by Cu- and Ni-rich factors (Fig. 3b) and their WCWT result (Fig. S5), high  $\text{PM}_{2.5}$  concentration in Stage 3 was attributed to long-range transportation from south China. Previous studies have also demonstrated the strong influence of air masses from southeast China on HCMC (Huy et al., 2022; Nguyen et al., 2023). The concentrations of  $\text{PM}_{2.5}$  from shipping emissions, coal combustion, and industrial

activities in China increased post-lockdown period (from the middle of February) (Cheng et al., 2022; Pei et al., 2022), which coincided with the lockdown period in HCMC. The  $PM_{2.5}$  mass in Stages 1, 2, and 4 might be emitted from domestic coal and crude oil combustion in the northeast/southwest direction of the sampling site. Hence, Cu- and Ni-rich factor is defined as long-range transport from coal and crude oil combustion and comprise 9% of the  $PM_{2.5}$  mass.

### 3.2.6 Minor sources

Soil dust emission is reflected in the high levels of Ca, Mg, Al, and Fe, which are generally considered indicators of soil dust (Reimann & De Caritat, 2000; Taylor, 1964). The annual contribution of soil dust to  $PM_{2.5}$  were 6%, 6%, 15%, and 8% during Stage 1–4, respectively, with an annual average contribution of 8%. The high correlation between Ca, Mg, and Al (Table 1,  $r > 0.85$ ,  $p < 0.01$ ) demonstrated that they originate from the same source during the sampling period. The high concentration of Al in this study agrees well with previous studies in Vietnam (Hien et al., 2022; Vuong et al., 2023). The significant contribution of soil dust during Stage 3 remains unclear; however, a reduction in human activities due to ARL could be the cause for minor sources of  $PM_{2.5}$  becoming more prominent in the HCMC.

Mn-rich source is represented by the highest loading of Mn (~79%), constituting ~4.3%  $PM_{2.5}$  in HCMC. Sources of Mn emissions include sand mining (Bari & Kindzierski, 2017), abrasion (road dust and tire wear) (Bressi et al., 2014; Jeong et al., 2022), and other natural processes (soil erosion, volcanic activity, and excavation) (Fakhri et al., 2023). The EF values of Mn were below 10, indicating Mn to have crustal origins. Therefore, the impact of abrasion emissions can be neglected. However, the contribution of Mn-rich sources to  $PM_{2.5}$  poses a discrepancy with the contribution of anthropogenic-rich sources, suggesting nonlocal origins for this source. Notably, sand mining activities in the Mekong Delta have increased in recent years (Jordan et al., 2019) leading to challenges, such as coastal erosion and airborne Mn emissions. Consequently, these factors should be carefully considered in developing future air quality management efforts.

The Pb-rich source was characterized by high levels of Pb (~81%), contributing a very small portion (< 1%) to the total  $PM_{2.5}$  concentrations. The mean EFs of Pb exceeded 10 in Stages 1, 2, and 4, compared to Stages 3, where it was lower than 10. Thus, Pb was considered derived from natural and anthropogenic sources. Additionally, it showed a moderate correlation with  $K^+$  ( $r = 0.554$ ,  $p < 0.01$ ), suggesting that Pb emissions may be related to combustion activities.

### 3.3 WCWT analysis

Figure 4 illustrates clusters of backward trajectories categorized by the four stages. During Stage 1, two of the main trajectories observed were originating from the northeast (~68%), while the other two clusters originated from the south (~16%) and southwest (~16%). In addition, 100% of the cluster patterns were distributed in the northeast regions during Stage 2 and Stage 3. Meanwhile, most of the clusters were derived from the south and southwest (~78%) and eastern regions (~12%) during Stage 4.

Herein, we utilized WCWT analysis to investigate the geological source of each component, which involved integrating the PMF-derived  $PM_{2.5}$  concentrations with the backward trajectories. Figure 5 indicates the transport pattern in the whole sampling period, while Figs. S5, S6, S7, S8, S9, S10, S11, S12 illustrate the transport pattern for each state of each source. Based on the WCWT analysis,  $PM_{2.5}$  emission sources were in the center of HCMC and were majorly scattered to the northeast area of this region (Fig. 5). These results are consistent with previous studies in HCMC (Bui et al., 2023; Hien et al., 2022; Huy et al., 2022; Tran et al., 2023). For instance, Hien et al. (2022) and Bui et al. (2023) suggested that long-range transport from coal-fired thermal plants in northeastern HCMC and in south China is reflected through the presence of As and Pb in HCMC. In addition, the presence of As in HCMC may specifically be related to emissions from Bien Hoa City (BHC). BHC is a hotspot of industrial establishment and is located about 35 km to the northeast of the sampling site. Bui et al. (2023) reported that the sources of As were closely related to coal combustion, industrial emissions, and processes involving excavating and treating contaminated soil. The occurrence of As in HCMC is a serious concern as it is a carcinogen responsible for posing 10% of the total carcinogenic risk in HCMC (Hien et al., 2022).

The influence of coal and crude oil combustion was clearly observed during Stage 3 (Fig. S5) when local anthropogenic emissions were largely minimized. The Mn-rich source was associated with air masses originating from south/southwest HCMC, supporting our suggestion that it could be a result of Mn emissions from sand mining in the Mekong Delta (Fig. S6). The road dust source represented by Zn demonstrated a similar pattern to previous studies, implying that long-range transport from the Philippines is a potential Zn source (Bui et al., 2023; Hien et al., 2022). In this study, the long-range transport from surrounding regions of HCMC and neighboring countries was observed to play an important role in the high concentration of  $PM_{2.5}$  and thus cannot be neglected.

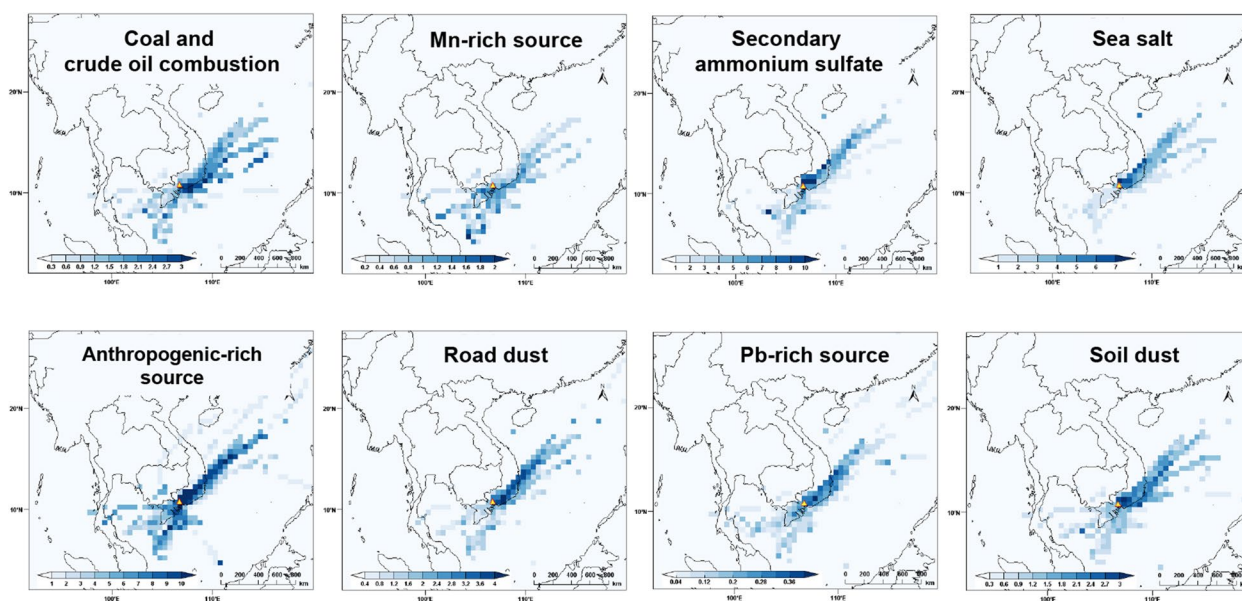


**Fig. 5** WCWT analysis based on PMF 5.0 results. The unit of the WCWT value:  $\mu\text{g m}^{-3}$

#### 4 Conclusion

The ambient  $\text{PM}_{2.5}$  samples were collected from HCMC between 2019 and 2020 to identify the primary sources and geological origins of  $\text{PM}_{2.5}$ . The main conclusions are as follows:

1. The EFs of Al, Mn, V, Mg, Ca, and Fe were  $< 10$ , indicating that their primary contributor was the Earth's crust. The EFs of Cu, As, and Zn were  $> 10$ , implying a substantial anthropogenic contribution. The EFs of Ni and Cu were  $\sim 10$ , suggesting a contribution from both anthropogenic emissions and the Earth's crust.
2. The apportionment of the source of ambient  $\text{PM}_{2.5}$  in HCMC was estimated using PMF for the first time. The results of PMF indicated that the most significant contributor of  $\text{PM}_{2.5}$  in HCMC was anthropogenic-rich sources (36.4% of  $\text{PM}_{2.5}$  mass), comprising biomass burning, coal combustion, transportation, and crustal origins. Other secondary sources of  $\text{PM}_{2.5}$  were ammonium sulfate (18.4%), sea salt (13.7%), road dust (9.6%), and coal and crude oil combustion (9.4%). Soil dust, Mn-rich sources, and Pb-rich sources were minor contributors that accounted for 13.1% of the  $\text{PM}_{2.5}$  mass. The WCWT analysis combined the backward trajectories of air mass with  $\text{PM}_{2.5}$  mass attributed to each factor. The primary contribution of  $\text{PM}_{2.5}$  was observed in HCMC, whereas air masses originating from the northeast and southwest areas of HCMC were contributed by long-distance transport.

3. During the ARL, a considerable decrease in  $\text{PM}_{2.5}$  resulting from anthropogenic activities was documented, highlighting the substantial contribution of direct emissions from anthropogenic activities to ambient  $\text{PM}_{2.5}$  in urban areas. Furthermore, the influence of air masses from neighboring countries on HCMC was observed during this period.

#### Supplementary Information

The online version contains supplementary material available at <https://doi.org/10.1007/s44273-023-00024-7>.

**Additional file 1: Table S1.** Statistics of PMF 5.0 input data. **Table S2.** Mapping of bootstrap factors to base factors. **Fig. S1.** The accumulation (columns) and measurement (white dots) of  $\text{PM}_{2.5}$  concentration. **Fig. S2.** Regression coefficients between measured and PMF-calculated  $\text{PM}_{2.5}$  concentrations. **Fig. S3.** The time-series of  $\text{PM}_{2.5}$  concentration by each source emissions. **Fig. S4.** Time series of molar ratio of  $\text{Cl}^-$  to  $\text{Na}^+$ . **Fig. S5.** WCWT result of coal and crude oil combustion. The unit of the WCWT value:  $\mu\text{g m}^{-3}$ . **Fig. S6.** WCWT result of Mn-rich source. The unit of the WCWT value:  $\mu\text{g m}^{-3}$ . **Fig. S7.** WCWT result of secondary ammonium sulfate. The unit of the WCWT value:  $\mu\text{g m}^{-3}$ . **Fig. S8.** WCWT result of sea salt. The unit of the WCWT value:  $\mu\text{g m}^{-3}$ . **Fig. S9.** WCWT result of the anthropogenic-rich source. The unit of the WCWT value:  $\mu\text{g m}^{-3}$ . **Fig. S10.** WCWT result of road source. The unit of the WCWT value:  $\mu\text{g m}^{-3}$ . **Fig. S11.** WCWT result of Pb-rich source. The unit of the WCWT value:  $\mu\text{g m}^{-3}$ . **Fig. S12.** WCWT result of soil dust. The unit of the WCWT value:  $\mu\text{g m}^{-3}$ .

#### Acknowledgements

This work was supported by the Japan Science and Technology Agency 6 (JST)-SPRING Program (JPMJSP2139), the JSPS Kakenhi (grant number: 21K7896), and the Environment Research and Technology Development Fund (JPMEERF20215003) of the Environmental Restoration and Conservation Agency of Japan. We also appreciate the financial support from the

Vingroup Innovation Foundation (VINIF.2022.ThS.053). We thank Dr. Mohammad Moniruzzaman and the Bangladesh Council of Scientific and Industrial Research staffs for helping with the trace elements analysis.

#### Authors' contributions

Ngoc Tran: Conceptualization, methodology, validation, formal analysis, investigation, data curation, writing—original draft, and visualization. Yusuke Fujii: Conceptualization, methodology, formal analysis, resources, writing—review and editing, supervision, project administration, and funding acquisition. Md Firoz Khan: Methodology, formal analysis, and validation. To Thi Hien: Methodology, investigation, resources, and writing—review and editing. Tran Hoang Minh: Investigation and methodology. Hiroshi Okochi: Resources and funding acquisition. Norimichi Takenaka: Resources and writing—review and editing.

#### Availability of data and materials

The datasets generated during and/or analyzed during the current study are available from the corresponding author on reasonable request.

#### Declarations

#### Competing interests

The authors declare that they have no known competing financial interests or personal relationships that could have appeared to influence the work reported in this study.

#### Author details

<sup>1</sup>Department of Sustainable System Sciences, Graduate School of Humanities and Sustainable System Sciences, Osaka Prefecture University, Sakai, Osaka, Japan. <sup>2</sup>Division of Sustainable System Sciences, Graduate School of Sustainable System Sciences, Osaka Metropolitan University, Sakai, Osaka, Japan. <sup>3</sup>Department of Environmental Science and Management, North South University, Dhaka, Bangladesh. <sup>4</sup>Faculty of Environment, University of Science, Ho Chi Minh City, Vietnam. <sup>5</sup>Vietnam National University Ho Chi Minh City, Ho Chi Minh City, Vietnam. <sup>6</sup>School of Creative Science and Engineering, Waseda University, Shinjuku, Tokyo, Japan.

Received: 18 September 2023 Accepted: 11 December 2023

Published online: 02 January 2024

#### References

- Ali-Taleshi, M. S., Moenaddini, M., Riyahi Bakhtiari, A., Feiznia, S., Squizzato, S., & Bourliva, A. (2021). A one-year monitoring of spatiotemporal variations of PM<sub>2.5</sub>-bound PAHs in Tehran, Iran: Source apportionment, local and regional sources origins and source-specific cancer risk assessment. *Environmental Pollution*, *274*, 115883. <https://doi.org/10.1016/j.envpol.2020.115883>
- Alias, N. F., Khan, M. F., Sairi, N. A., Zain, S. M., Suradi, H., Ab Rahim, H. A., Banerjee, T., Bari, M. A., Othman, M., & Latif, M. T. (2020). Characteristics, emission sources, and risk factors of heavy metals in PM<sub>2.5</sub> from Southern Malaysia. *ACS Earth and Space Chemistry*, *4*(8), 1309–1323. <https://doi.org/10.1021/acsearthspacechem.0c00103>
- Bari, M. A., & Kindzierski, W. B. (2017). Ambient fine particulate matter (PM<sub>2.5</sub>) in Canadian oil sands communities: levels, sources and potential human health risk. *Science of The Total Environment*, *595*, 828–838. <https://doi.org/10.1016/j.scitotenv.2017.04.023>
- Boreddy, S. K. R., Kawamura, K., & Jung, J. (2014). Hygroscopic properties of particles nebulized from water extracts of aerosols collected at Chichijima Island in the western North Pacific: an outflow region of Asian dust. *Journal of Geophysical Research*, *119*(1), 167–178. <https://doi.org/10.1002/2013JD020626>
- Bressi, M., Sciare, J., Gherzi, V., Mihalopoulos, N., Petit, J.-E., Nicolas, J. B., Moukhtar, S., Rosso, A., Féron, A., Bonnaire, N., Poulakis, E., & Theodosi, C. (2014). Sources and geographical origins of fine aerosols in Paris (France). *Atmospheric Chemistry and Physics*, *14*, 8813–8839. <https://doi.org/10.5194/acp-14-8813-2014>
- Bui, D. L., Hoang, A. L., Ngo, Q. K., & Nghiem, X. T. (2023). Chemical characterization, source apportionment, and health risk assessment nexus of PM<sub>2.5</sub>-bound major heavy metals in Bien Hoa city, southern Vietnam. *Atmospheric Environment: X*, *17*, 100209. <https://doi.org/10.1016/j.aeaoo.2023.100209>
- Chen, T., Liu, Y., Ma, Q., Chu, B., Zhang, P., Liu, C., Liu, J., & He, H. (2019). Significant source of secondary aerosol: formation from gasoline evaporative emissions in the presence of SO<sub>2</sub> and NH<sub>3</sub>. *Atmospheric Chemistry and Physics*, *19*(12), 8063–8081. <https://doi.org/10.5194/acp-19-8063-2019>
- Cheng, K., Chang, Y., Kuang, Y., Khan, R., & Zou, Z. (2022). Elucidating the responses of highly time-resolved PM<sub>2.5</sub> related elements to extreme emission reductions. *Environmental Research*, *206*, 112624. <https://doi.org/10.1016/j.envres.2021.112624>
- Chifang, C., Zhuguo, D., Jiamo, F., & Guoying, S. (1991). Determination of trace elements in crude oils and organic materials extracted from oil-forming source rocks in China by INAA. *Journal of Radioanalytical and Nuclear Chemistry*, *151*(1), 177–84. <https://doi.org/10.1007/BF02040144>
- Cui, Y., Ji, D., Maenhaut, W., Gao, W., Zhang, R., & Wang, Y. (2020). Levels and sources of hourly PM<sub>2.5</sub>-related elements during the control period of the COVID-19 pandemic at a rural site between Beijing and Tianjin. *Science of the Total Environment*, *744*, 140840. <https://doi.org/10.1016/j.scitotenv.2020.140840>
- Dahari, N., Muda, K., Latif, M. T., & Hussein, N. (2019). Studies of atmospheric PM<sub>2.5</sub> and its inorganic water soluble ions and trace elements around Southeast Asia: a review. *Asia-Pacific Journal of Atmospheric Sciences*, *57*(2), 361–385. <https://doi.org/10.1007/S13143-019-00132-X>
- Dai, W., Gao, J., Cao, G., & Ouyang, F. (2013). Chemical composition and source identification of PM<sub>2.5</sub> in the suburb of Shenzhen. *China Atmospheric Research*, *122*, 391–400. <https://doi.org/10.1016/j.atmosres.2012.12.004>
- Fakhri, Y., Akhlaghi, M., Daraei, H., Hedarinejad, Z., Bahreini, A., Mahmudiono, T., & Mousavi Khaneghah, A. (2023). The concentration of potentially toxic elements (zinc, iron, manganese) bound PM<sub>2.5</sub> in the indoor air of urban schools: a global systematic review and meta-analysis. *Air Quality, Atmosphere and Health*, *16*(1), 77–84. <https://doi.org/10.1007/s11869-022-01257-1>
- Farren, N. J., Dunmore, R. E., Mead, M. I., Nadzir, M. S. M., Samah, A. A., Phang, S. M., Bandy, B. J., Sturges, W. T., & Hamilton, J. F. (2019). Chemical characterisation of water-soluble ions in atmospheric particulate matter on the east coast of Peninsular Malaysia. *Atmospheric Chemistry and Physics*, *19*(3), 1537–1553. <https://doi.org/10.5194/ACP-19-1537-2019>
- Fujii, Y., Tohno, S., Amil, N., & Latif, M. T. (2017). Quantitative assessment of source contributions to PM<sub>2.5</sub> on the west coast of Peninsular Malaysia to determine the burden of Indonesian peatland fire. *Atmospheric Environment*, *171*, 111–117. <https://doi.org/10.1016/j.atmosenv.2017.10.009>
- Fujii, Y., Mahmud, M., Tohno, S., Okuda, T., & Mizohata, A. (2016). A case study of PM<sub>2.5</sub> characterization in Bangi, Selangor, Malaysia during the southwest monsoon season. *Aerosol and Air Quality Research*, *16*(11), 2685–2691. <https://doi.org/10.4209/aaqr.2015.04.0277>
- Gunawardena, J., Egodawatta, P., Ayoko, G. A., & Goonetilleke, A. (2013). Atmospheric deposition as a source of heavy metals in urban stormwater. *Atmospheric Environment*, *68*, 235–242. <https://doi.org/10.1016/j.atmosenv.2012.11.062>
- Hao, Y., Meng, X., Yu, X., Lei, M., Li, W., Shi, F., Yang, W., Zhang, S., & Xie, S. (2018). Characteristics of trace elements in PM<sub>2.5</sub> and PM<sub>10</sub> of Chifeng, northeast China: insights into spatiotemporal variations and sources. *Atmospheric Research*, *213*, 550–561. <https://doi.org/10.1016/j.atmosres.2018.07.006>
- Hien, T. T., Chi, N. D. T., Huy, D. H., Le, H. A., Oram, D. E., Forster, G. L., Mills, G. P., & Baker, A. R. (2022). Soluble trace metals associated with atmospheric fine particulate matter in the two most populous cities in Vietnam. *Atmospheric Environment: X*, *15*, 100178. <https://doi.org/10.1016/j.aeaoo.2022.100178>
- Hien, T. T., Chi, N. D. T., Nguyen, N. T., Vinh, L. X., Takenaka, N., & Huy, D. H. (2019). Current status of fine particulate matter (PM<sub>2.5</sub>) in Vietnam's most populous city, Ho Chi Minh City. *Aerosol and Air Quality Research*, *19*(10), 2239–2251. <https://doi.org/10.4209/aaqr.2018.12.0471>
- Ho, B. Q., & Clappier, A. (2011). Road traffic emission inventory for air quality modelling and to evaluate the abatement strategies: a case of Ho Chi Minh City Vietnam. *Atmospheric Environment*, *45*(21), 3584–3593. <https://doi.org/10.1016/j.atmosenv.2011.03.073>
- Ho, B. Q., Vu, K. H. N., Nguyen, T. T., Nguyen, H. T. T., Ho, D. M., Nguyen, H. N., & Nguyen, T. T. T. (2020). Study loading capacities of air pollutant emissions for developing countries: a case of Ho Chi Minh City. *Vietnam. Scientific Reports*, *10*, 5827. <https://doi.org/10.1038/s41598-020-62053-4>

- Hong Phuong, P. T., Nghiem, T. D., Mai Thao, P. T., & Nguyen, T. D. (2022). Emission factors of selected air pollutants from rice straw open burning in the Mekong Delta of Vietnam. *Atmospheric Pollution Research*, 13(3), 101353. <https://doi.org/10.1016/j.apr.2022.101353>
- Hsu, Y. K., Holsen, T. M., & Hopke, P. K. (2003). Comparison of hybrid receptor models to locate PCB sources in Chicago. *Atmospheric Environment*, 37(4), 545–562. [https://doi.org/10.1016/S1352-2310\(02\)00886-5](https://doi.org/10.1016/S1352-2310(02)00886-5)
- Hu, G. P., & Balasubramanian, R. (2003). Wet deposition of trace metals in Singapore. *Water, Air, and Soil Pollution*, 144, 285–300. <https://doi.org/10.1023/A:1022921418383>
- Huong Giang, N. T., & Kim Oanh, N. T. (2014). Roadside levels and traffic emission rates of PM<sub>2.5</sub> and BTEX in Ho Chi Minh City. *Vietnam. Atmospheric Environment*, 94, 806–816. <https://doi.org/10.1016/j.atmosenv.2014.05.074>
- Huy, D. H., Thanh, L. T., Hien, T. T., & Takenaka, N. (2020). Comparative study on water-soluble inorganic ions in PM<sub>2.5</sub> from two distinct climate regions and air quality. *Journal of Environmental Sciences (China)*, 88, 349–360. <https://doi.org/10.1016/j.jes.2019.09.010>
- Huy, D. H., Hien, T. T., & Takenaka, N. (2022). Influence of urban outflow on water-soluble ions in PM<sub>2.5</sub> and > PM<sub>2.5</sub> particles at a suburban Ho Chi Minh City site, Vietnam. *Atmospheric Research*, 272, 106144. <https://doi.org/10.1016/j.atmosres.2022.106144>
- Huyen, T. T., Oanh, N. T. K., Huy, L. N., Winiukul, E., & Chi, N. N. H. (2022). Impact of lowering fuel sulfur content on atmospheric emissions from shipping activities in a World Heritage Bay in Vietnam. *Environmental Technology & Innovation*, 27, 102507. <https://doi.org/10.1016/j.eti.2022.102507>
- Jeong, C. H., Yousif, M., & Evans, G. J. (2022). Impact of the COVID-19 lockdown on the chemical composition and sources of urban PM<sub>2.5</sub>. *Environmental Pollution*, 292, 118417. <https://doi.org/10.1016/j.envpol.2021.118417>
- Jordan, C., Tiede, J., Lojek, O., Visscher, J., Apel, H., Quan Nguyen, H., Nguyen, C., Quang, X., & Schlurmann, T. (2019). Sand mining in the Mekong Delta revisited-current scales of local sediment deficits. *Scientific Report*, 9, 17823. <https://doi.org/10.1038/s41598-019-53804-z>
- Khamkaew, C., Chantara, S., Janta, R., Pani, S. K., Prapamontol, T., Kawichai, S., Wiriy, W., & Lin, N. H. (2016). Investigation of biomass burning chemical components over Northern Southeast Asia during 7-SEAS/BASELInE 2014 campaign. *Aerosol and Air Quality Research*, 16, 2655–2670. <https://doi.org/10.4209/aaqr.2016.03.0105>
- Khan, M. F., Latif, M. T., Saw, W. H., Amil, N., Nadzir, M., Sahani, M., Tahir, N. M., & Chung, J. X. (2016). Fine particulate matter in the tropical environment: monsoonal effects, source apportionment, and health risk assessment. *Atmospheric Chemistry and Physics*, 16, 597–617. <https://doi.org/10.5194/acp-16-597-2016>
- Kopplitz, S. N., Jacob, D. J., Sulprizio, M. P., Myllyvirta, L., & Reid, C. (2017). Burden of disease from rising coal-fired power plant emissions in Southeast Asia. *Environmental Science and Technology*, 51(3), 1467–1476. <https://doi.org/10.1021/acs.est.6b03731>
- Ledoux, F., Kfoury, A., Delmaire, G., Roussel, G., El Zein, A., & Courcot, D. (2017). Contributions of local and regional anthropogenic sources of metals in PM<sub>2.5</sub> at an urban site in northern France. *Chemosphere*, 181, 713–724. <https://doi.org/10.1016/j.chemosphere.2017.04.128>
- Li, R., Li, J., Cui, L., Wu, Y., Fu, H., Chen, J., & Chen, M. (2017). Atmospheric emissions of Cu and Zn from coal combustion in China: spatio-temporal distribution, human health effects, and short-term prediction. *Environmental Pollution*, 229, 724–734. <https://doi.org/10.1016/j.envpol.2017.05.068>
- Li, X., Yan, C., Wang, C., Ma, J., Li, W., Liu, J., & Liu, Y. (2022). PM<sub>2.5</sub>-bound elements in Hebei Province, China: pollution levels, source apportionment and health risks. *Science of The Total Environment*, 806, 150440. <https://doi.org/10.1016/j.scitotenv.2021.150440>
- Liu, B., Wu, J., Zhang, J., Wang, L., Yang, J., Liang, D., Dai, Q., Bi, X., Feng, Y., Zhang, Y., & Zhang, Q. (2017). Characterization and source apportionment of PM<sub>2.5</sub> based on error estimation from EPA PMF 5.0 model at a medium city in China. *Environmental Pollution*, 222, 10–22. <https://doi.org/10.1016/j.envpol.2017.01.005>
- Long, S., Zeng, J., Li, Y., Bao, L., Cao, L., Liu, K., Xu, L., Lin, J., Liu, W., Wang, G., Yao, J., Ma, C., & Zhao, Y. (2014). Characteristics of secondary inorganic aerosol and sulfate species in size-fractionated aerosol particles in Shanghai. *Journal of Environmental Sciences (China)*, 26(5), 1040–1051. [https://doi.org/10.1016/S1001-0742\(13\)60521-5](https://doi.org/10.1016/S1001-0742(13)60521-5)
- Luong, N. D., Hieu, B. T., Trung, B. Q., Van Dat, M., Van Duy, N., Van Dinh, P., Hien, T. T., & Hiep, N. H. (2022). Investigation of sources and processes influencing variation of PM<sub>2.5</sub> and its chemical compositions during a summer period of 2020 in an urban area of Hanoi city. *Vietnam. Air Quality, Atmosphere and Health*, 15, 235–253. <https://doi.org/10.1007/s11869-021-01100-z>
- Makkonen, U., Vestenius, M., Huy, L. N., Anh, N. T. N., Linh, P. T. V., Thuy, P. T., Phuong, H. T. M., Nguyen, H., Thuy, L. T., Aurela, M., Hellén, H., Lovén, K., Kouznetsov, R., Kyllönen, K., Teinilä, K., & Kim Oanh, N. T. (2023). Chemical composition and potential sources of PM<sub>2.5</sub> in Hanoi. *Atmospheric Environment*, 299, 119650. <https://doi.org/10.1016/j.atmosenv.2023.119650>
- Manousakas, M., Papaefthymiou, H., Diapouli, E., Migliori, A., Karydas, A. G., Bogdanovic-Radovic, I., & Eleftheriadis, K. (2017). Assessment of PM<sub>2.5</sub> sources and their corresponding level of uncertainty in a coastal urban area using EPA PMF 5.0 enhanced diagnostics. *Science of the Total Environment*, 574, 155–164. <https://doi.org/10.1016/j.scitotenv.2016.09.047>
- Nayebare, S. R., Aburizaiza, O. S., Siddique, A., Carpenter, D. O., Hussain, M. M., Zeb, J., Aburizaiza, A. J., & Khwaja, H. A. (2018). Ambient air quality in the holy city of Makkah: a source apportionment with elemental enrichment factors (EFs) and factor analysis (PMF). *Environmental Pollution*, 243, 1791–1801. <https://doi.org/10.1016/j.envpol.2018.09.086>
- Nguyen, T. P. M., Bui, T. H., Nguyen, M. K., Nguyen, T. H., Vu, V. T., & Pham, H. L. (2022). Impact of COVID-19 partial lockdown on PM<sub>2.5</sub>, SO<sub>2</sub>, NO<sub>2</sub>, O<sub>3</sub>, and trace elements in PM<sub>2.5</sub> in Hanoi, Vietnam. *Environmental Science and Pollution Research International*, 29(28), 41875–41885. <https://doi.org/10.1007/s11356-021-13792-y>
- Nguyen, T. N. T., Du, N. X., & Hoa, N. T. (2023). Emission source areas of fine particulate matter (PM<sub>2.5</sub>) in Ho Chi Minh City, Vietnam. *Atmosphere*, 14(3), 579. <https://doi.org/10.3390/ATMOS14030579/S1>
- Norris, G., Duvall, R., Brown, S., & Bai, S. (2014). EPA Positive Matrix Factorization (PMF) 5.0 fundamentals and user guide. U.S. Environmental Protection Agency, Washington, DC. EPA/600/R-14/108 (NTIS PB2015-105147)
- Paatero, P., & Tapper, U. (1994). Positive matrix factorization: a non-negative factor model with optimal utilization of error estimates of data values. *Environmetrics*, 5, 111–126. <https://doi.org/10.1002/env.3170050203>
- Pei, C., Yang, W., Zhang, Y., Song, W., Xiao, S., Wang, J., Zhang, J., Zhang, T., Chen, D., Wang, Y., Chen, Y., & Wang, X. (2022). Decrease in ambient volatile organic compounds during the COVID-19 lockdown period in the Pearl River Delta region, south China. *Science of The Total Environment*, 823, 153720. <https://doi.org/10.1016/j.scitotenv.2022.153720>
- Reimann, C., & De Caritat, P. (2000). Intrinsic flaws of element enrichment factors (EFs) in environmental geochemistry. *Environmental Science and Technology*, 34(24), 5084–5091. <https://doi.org/10.1021/es001339o>
- Taghvaei, S., Sowlat, M. H., Mousavi, A., Hassanvand, M. S., Yunesian, M., Naddafi, K., & Sioutas, C. (2018). Source apportionment of ambient PM<sub>2.5</sub> in two locations in central Tehran using the Positive Matrix Factorization (PMF) model. *Science of the Total Environment*, 628–629(1547), 672–686. <https://doi.org/10.1016/j.scitotenv.2018.02.096>
- Taylor, S. R. (1964). Abundance of chemical elements in the continental crust: a new table. *Geochimica et Cosmochimica Acta*, 28(8), 1273–1285. [https://doi.org/10.1016/0016-7037\(64\)90129-2](https://doi.org/10.1016/0016-7037(64)90129-2)
- Tran, N., Fujii, Y., Le, V. X., Doan, N., Chi, T., Okochi, H., Hien, T. T., & Takenaka, N. (2023). Annual variation of PM<sub>2.5</sub> chemical composition in Ho Chi Minh City, Vietnam including the COVID-19 outbreak period. *Aerosol and Air Quality Research*, 23(5), 220312. <https://doi.org/10.4209/aaqr.220312>
- Vuong, Q. T., Bac, V. T., Thang, P. Q., Park, M. K., & Choi, S. D. (2023). Trace element characterization and source identification of particulate matter of different sizes in Hanoi Vietnam. *Urban Climate*, 48, 101408. <https://doi.org/10.1016/j.uclim.2023.101408>
- Wang, Y. Q., Zhang, X. Y., & Draxler, R. R. (2009). TrajStat: GIS-based software that uses various trajectory statistical analysis methods to identify potential sources from long-term air pollution measurement data. *Environmental Modelling and Software*, 24(8), 938–939. <https://doi.org/10.1016/j.envsoft.2009.01.004>
- Wang, B., Li, Y., Tang, Z., Cai, N., Zhang, N., & Liu, J. (2021). The heavy metals in indoor and outdoor PM<sub>2.5</sub> from coal-fired and non-coal-fired area. *Urban Climate*, 40, 101000. <https://doi.org/10.1016/j.uclim.2021.101000>
- Xue, J., Yuan, Z., Lau, A. K. H., & Yu, J. Z. (2014). Insights into factors affecting nitrate in PM<sub>2.5</sub> in a polluted high NO<sub>x</sub> environment through hourly observations and size distribution measurements. *Journal of Geophysical Research: Atmospheres*, 119(8), 4888–4902. <https://doi.org/10.1002/2013JD021108>

- Yan, Q., Kong, S., Yan, Y., Liu, X., Zheng, S., Qin, S., Wu, F., Niu, Z., Zheng, H., Cheng, Y., Zeng, X., Wu, J., Yao, L., Liu, D., Shen, G., Shen, Z., & Qi, S. (2022). Emission and spatialized health risks for trace elements from domestic coal burning in China. *Environment International*, 158, 107001. <https://doi.org/10.1016/j.envint.2021.107001>
- Yang, D., Ye, C., Wang, X., Lu, D., Xu, J., & Yang, H. (2018). Global distribution and evolution of urbanization and PM<sub>2.5</sub> (1998–2015). *Atmospheric Environment*, 182, 171–178. <https://doi.org/10.1016/j.atmosenv.2018.03.053>
- Yin, S., Wang, X., Zhang, X., Guo, M., Miura, M., & Xiao, Y. (2019). Influence of biomass burning on local air pollution in mainland Southeast Asia from 2001 to 2016. *Environmental Pollution*, 254, 112949. <https://doi.org/10.1016/j.envpol.2019.07.117>
- Zhang, Y., Yang, L., Bie, S., Zhao, T., Huang, Q., Li, J., Wang, P., Wang, Y., & Wang, W. (2021). Chemical compositions and the impact of sea salt in atmospheric PM<sub>1</sub> and PM<sub>2.5</sub> in the coastal area. *Atmospheric Research*, 250, 105323. <https://doi.org/10.1016/j.atmosres.2020.105323>
- Zhao, C., & Luo, K. (2018). Household consumption of coal and related sulfur, arsenic, fluorine and mercury emissions in China. *Energy Policy*, 112, 221–232. <https://doi.org/10.1016/J.ENPOL.2017.10.021>
- Zhuang, B., Wang, T., Liu, J., Li, S., Xie, M., Han, Y., Chen, P., Hu, Q., Yang, X. Q., Fu, C., & Zhu, J. (2017). The surface aerosol optical properties in the urban area of Nanjing, west Yangtze River Delta China. *Atmospheric Chemistry and Physics*, 17(2), 1143–1160. <https://doi.org/10.5194/acp-17-1143-2017>
- Zong, Z., Wang, X., Tian, C., Chen, Y., Fu, S., Qu, L., Ji, L., Li, J., & Zhang, G. (2018). PMF and PSCF based source apportionment of PM<sub>2.5</sub> at a regional background site in North China. *Atmospheric Research*, 203, 207–215. <https://doi.org/10.1016/j.atmosres.2017.12.013>

### Publisher's Note

Springer Nature remains neutral with regard to jurisdictional claims in published maps and institutional affiliations.